EDN: RULPRP
УДК 535.8

Simulation of Single-Pixel Camera Method Application for mapping the Spatial Layout of Objects in LIDAR Technologies

Anastasiia K. Lappo-Danilevskaia*
Azat O. Ismagilov†
ITMO University
Saint-Petersburg, Russian Federation
Aleksei A. Kalinichev ‡
Saint-Petersburg State University
Saint-Petersburg, Russian Federation
Anton N. Tcypkin§
ITMO University
Saint-Petersburg, Russian Federation

Received 27.10.2024, received in revised form 13.12.2024, accepted 14.01.2025

Abstract. This work presents the simulation results demonstrating the successful application of single-pixel imaging for the reconstruction of three-dimensional object images, in combination with LIDAR technologies. Specifically, the integration of pulsed radiation-based Time of Flight (ToF) and Frequency Modulated Continuous Wave (FMCW) LIDAR methods is explored. In the case of ToF, the simulations reveal enhanced accuracy in distinguishing distances between objects that are smaller than the distance light travels in half the duration of the scanning pulse. These findings highlight the potential of single-pixel imaging in advanced 3D visualization and distance measurement applications.

Keywords: Single pixel camera, 3D visualisation, Time of flight LIDAR, Frequency-modulated continious vawe LIDAR

Citation: A.K. Lappo-Danilevskaia, A.O. Ismagilov, A.A. Kalinichev, A.N. Tcypkin, Simulation of Single-Pixel Camera Method Application for mapping the Spatial Layout of Objects in LIDAR Technologies, J. Sib. Fed. Univ. Math. Phys., 2025, 18(3), 377–386. EDN: RULPRP.

With the active development of autonomous vehicles, robotics, digitalization of the urban environment, and the spread of smart home technology, object recognition, visualization, and location detection systems are becoming key elements to ensure more advanced, secure, high-precision implementations that can adapt to changing conditions. One of the popular methods currently in use is LIDAR — a technology that stands for "Light Detection and Ranging". LIDAR technologies are actively used for autonomous navigation [1], environmental monitoring [2], for autonomous and safe precision landing on solar system bodies [3], service robots [4], odometry and geospatial mapping [5]. Despite significant progress in remote 3D visualization, current methods are limited by either detection range or application mode limitations.

The principle of distance measurement in LIDARs can be classified based on the type of the source. Pulsed illumination is used in the Time of Flight (TOF) technique, where the distance is calculated by measuring the time it takes for light to return from the object. Continuous frequency-modulated signal is used in Frequency Modulated Continuous Wave (FMCW)

*ankonstld@itmo.ru https://orcid.org/0000-0002-1762-2688
† https://orcid.org/0000-0002-5844-2966
‡ https://orcid.org/0000-0001-8242-9457
§ https://orcid.org/0000-0002-9254-1116

LIDAR systems, where the distance is determined using the beat frequency between the initial and reflected from the object signals. Such techniques can be combined with different imaging principles.

One of them is raster scanning. For example, advantages of TOF-systems with raster scanning are a high resolution and long detection range due to the use of short pulses with high peak power. Notably, the reconstruction of a scene consisting of $n \times n \times n$ pixels takes n^2 measurements. Accordingly, there is a task of reducing the number of measurements while maintaining quality, as, for example, increasing the image speed is important for visualizing moving targets. Another implementation is a Flash camera that illuminates the entire field of view. Flash cameras utilize a matrix of detectors, raising concerns related to increasing quality and distance range. The cost associated with resolution enhancements can prove to be exorbitant when employing detector matrices.

As an alternative can be considered single-pixel imaging (SPI) techniques. Single pixel imaging has found applications in various fields, showcasing its versatility and potential impact. Some notable applications are Terahertz imaging [7, 8], X-ray imaging [9], where is a lack of detectors with spatial resolution, remote sensing [10], microscopy [11], imaging in low light [12] and noisy environments [13]. Instead of capturing the entire image at once, SPI relies on illuminating the object with a series of known, structured light patterns. For each pattern, the light transmitted or reflected by the object is collected by a single-pixel detector (sometimes called a "bucket detector"), which measures the total intensity of light, without any spatial information. The modulator position in the setup determines the setup configuration. In the case when the modulator stays between the object and illumination source, the technique names as a ghost imaging (GI) [14]. Currently from single-pixel technologies, the use of ghost imaging to improve LIDAR technology has been investigated and has shown both distance improvement and reconstruction speed increase [15–17].

Another approach is a single pixel camera method (SPC) that is based on structured detection [18]. This method achieves higher quality of the reconstructed image with an increased distance compared to the Ghost Imaging (GI) methods. This difference in quality can be attributed to the contributions of the optical setup elements [19]. This shows the possibility of obtaining better results when using the SPC method in lidar technologies compared to the GI.

In this work, SPC approach as a a method for obtaining information about the spatial distribution of objects was studied in combination with Time-of-Flight and Frequency modulated continuous wave LIDAR technologies for three-dimensional Objects Image Reconstruction.

1. Methods

The simulation was conducted in a Matlab Software Package. The propagation of the spatial distribution of radiation is considered using the example of the TOF configuration presented in the Fig. 1a. Simulation of the spatial profile of radiation includes calculating the field in the plane in front of the object $E_0(x, y, t)$, its interaction with objects $T(x, y, t)$, propagation of the interacted radiation to the DMD and its modulation by patterns.

The distribution of the field in the cross-section was given in the Gauss form according to [20]. The time distribution of pulses also took the form of a Gaussian distribution. The interaction of the spatial profile with the objects with transfer function $T(x, y, t)$ is calculated as follows: $E(x, y, t) = E_0(x, y, t) \times T(x, y, t)$. Propagation of whole reflected light to the DMD and all transmitted light to the next objects were made via angular spectrum approach [21].

The pulse $E_{beforeDMD}(x, y, t)$, which came to the spatial light modulator, is modulated by the mask $P_i(x, y)$ at each moment of time. After that, the integral intensity of the modulated radiation coming to the detector is calculated:

$$B_i(t) = \sum_{n=1}^{N_T} \iint E_{beforeDMDn}(x, y, t) \cdot P_i \cdot \cos\left(\varphi(x, y)\right) dxdy, \tag{1}$$

$$\varphi(x, y) = \arctan\left(\frac{\sqrt{x^2 + y^2}}{R_n}\right), \tag{2}$$

where $\varphi(x, y)$ is the solid angle between the target points and detector.

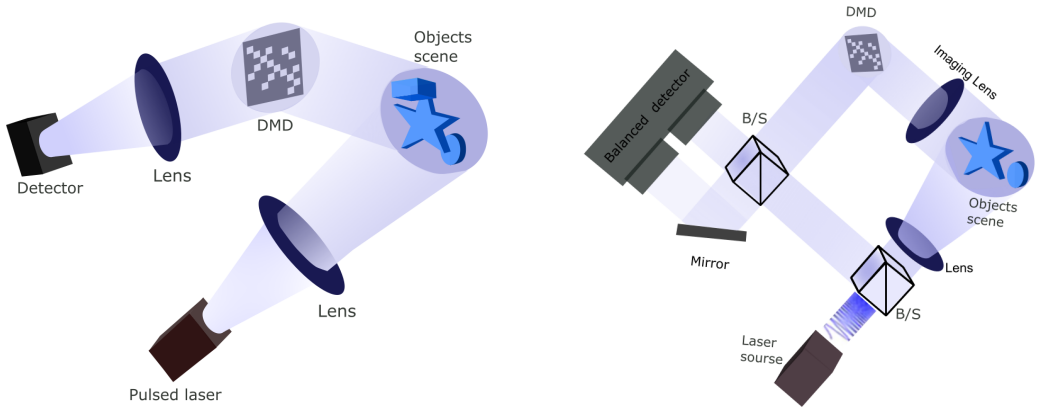

(a) (b)

Fig. 1. A schematic diagram of (a)SPC TOF LIDAR. A pulsed radiation source illuminates the scene with the object, the light from the target reflects and goes to a DMD. Modulated radiation is collected on a single-pixel detector, (b) SPC FMCW LIDAR. Frequency chirped radiation passes through a beamsplitter. The small fraction acts as a local oscillator, another one goes to the target, reflects and passes to the DMD. After DMD object beam is combined with the LO signal on the beamsplitter and combined radiation is detected by a balanced detector

The selection of patterns plays a crucial role in SPI, as there are various options available. One approach is to utilize random patterns, which are particularly advantageous in image recognition tasks where the full set of patterns is unnecessary. This approach can significantly reduce the number of measurements, making the process faster and more efficient. However, achievement of high-precision image restoration still requires a large number of measurements [22]. Another option is to use Fourier patterns, although they involve gray-scale values, which adds complexity to their generation and projection when compared to binary Hadamard patterns [23]. At the same time, in order to obtain a correct image, there is no need to use the entire set of masks. There are proposed techniques that help to reduce the required number of patterns based on sorting the columns of the Hadamard matrix, vivid examples are cake-cutting basis sort [24] and russian dolls [25]. In simulation the Hadamard patterns were used, the P_i modulation pattern is a 256×256 pixel matrix. To reduce the computational complexity, the generated mask was 64×64 and was expanded in 4 times. Hadamard patterns were formed from the Hadamard matrix H_{2^n} of order $n = 6$. Initially, the elements of the matrix contain values (–1.1), however, only positive Hadamard patterns are used to restore the images, therefore the –1 value is changed to 0. The Single pixel image were reconstructed with the use of Hadamard patterns by the following formula for SPC approach:

$$G(x, y) = \frac{1}{N} \sum_{i=1}^{N} B_i P_{i,(x,y)}. \tag{3}$$

The quality assessment can be performed using the structural similarity index (SSIM), which

takes into account parameters such as luminance $l(x,y)$, contrast $c(x,y)$ and structure $s(x,y)$

$$SSIM(x,y) = [l(x,y)]^{\alpha} \cdot [c(x,y)]^{\beta} \cdot [s(x,y)]^{\gamma}, \tag{4}$$

where $\alpha = \beta = \gamma = 1$.

The Fig. 1b shows a schematic diagram on which the simulation of the implementation of FMCW SPC LIDAR based on heterodyne detection [26] was performed. Electric field of the initial laser radiation $E_{\text{modulated}}$ has a linear frequency chirp with the start frequency f_0 and the final f_{max} [27]:

$$E_{\text{modulated}}(t) = A \exp\left(2\pi i \left[f_0 + \frac{f_{max} - v_0}{2T} t\right] t\right), \tag{5}$$

where A is an amplitude, T is a period of modulation.

Signal splits on a beamsplitter, one part acts as a local oscillator $E_{LO} = E_{modulated}$ and another fraction goes to the object, reflects and asquires time delay τ. The object signal is modulated by spatial masks on the DMD. The spatial profile of radiation and its interaction with the DMD is simulated as in the TOF case.

On the second beam splitter, E_{sig} is combined with E_{LO} and then the combined signal is sent to the balanced photodetector. The signal on the balanced photodetector after filtering sum-frequency signal components looks like this [27]:

$$\begin{aligned} P_{\text{Scope}}(t) = \frac{\epsilon_0 c}{2} \Bigg(& \left| \frac{E_{\text{LO}}(t) + i \sum_j E_{\text{Sig}}(t - \tau_j) * P_R(t)}{\sqrt{2}} \right|^2 - \\ & - \left| \frac{i E_{\text{LO}}(t) + \sum_j E_{\text{Sig}}(t - \tau_j) * P_R(t)}{\sqrt{2}} \right|^2 \Bigg) = \\ & = \epsilon_0 c \sum_j A_{\text{LO}} A_j P_R(t) \sin\left(2\pi \frac{\Delta\nu \tau_j}{T} t + v_0 \tau_j - \frac{\Delta v}{2T} \tau_j^2\right). \end{aligned} \tag{6}$$

The received signal is amplified by the signal of the local oscillator, which is 2 orders of magnitude more intense and at the same time contains only the following frequencies, which are visible as peaks in the frequency spectrum after the Fourier transform $P_{\text{Scope}}(t)$:

$$v_j = \frac{v_0 \tau_j}{2T}. \tag{7}$$

They are used to calculate the distance

$$d_j = \frac{v_j T c}{2\Delta v} \tag{8}$$

the value of the peak is used to reconstruct an image of the object via SPI method.

2. Simulation results

The following parameters were used: $w_0 = 15mm$ is the waist radius of a laser beam, $\lambda = 1550\ nm$ — laser wavelength. The spatial distribution of objects is shown in the Fig. 2a. The size of the reconstructed images is 256×256 pixels or 0.04×0.04 m.

The single-pixel camera approach reconstructs the image that directly passed on the spatial modulator, that is the diffracted one. When the Hadamard patterns are used for image reconstruction due to the high accuracy and quality on reconstructed image the diffraction artefacts are clearly visible (Fig. 2b). This necessitates the back propagation by the angular spectrum

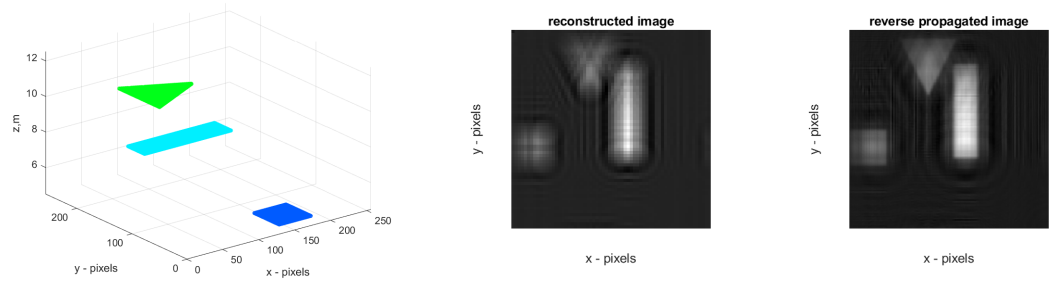

(a) (b) (c)

Fig. 2. (a) Object's spatial profile, (b) reconstructed image, (c) reverse propagated reconstructed image

method over a distance of $d_1 = \frac{t_1 c}{2}$, obtained using LIDAR technology. In the image obtained with its help, objects become clearly visible (Fig. 2c).

The temporal profile of the radiation was simulated with the following parameters: standard deviation $\sigma = 1.2 \times 10^{-9}$ and $FWHM = 2.8$ ns. This parameter determines the distance that can be distinguished using the TOF technique and it is determined by the response time of the detector. The time resolution of detected signal is controlled by an oscilloscope. On the market are presented oscilloscopes with following sampling rate: 2,5 GSa/s (Rohde Schwarz RTM3004), 8 GSa/s (RIGOL MSO5104), up to the 4 GSa/s (GW Instek GDS-73504A). 4 GSa/s was selected which corresponds to the time step 1 ps. The sampling rate F_s directly affects the resolution of the distance $\delta R = \frac{c}{2F_s}$.

Globally, the time profiles of reflected signals can be divided into two cases: objects are too close and the signals overlap into one indistinguishable peak (Fig. 3a) and objects are at a sufficient distance for the reflected signals to be resolved by the detection system (Fig. 4a). Using single-pixel imaging, it is possible to restore the image of objects at each discretized point, build depth maps of objects using them, take the average distance at which the object is distinguishable and thereby improve the quality of distance determination.

As an illustration of the construction of three-dimensional depth maps, two-dimensional reconstructed images were taken, restored at each discretized time point with a signal intensity above 20 %. After isolating objects from noise, the objects were built at a certain distance FROM LIDAR technology, forming a three-dimensional map of the objects.

To evaluate the determination of distances using TOF LIDAR technology and using reconstructed depth maps, error functions were constructed, calculated as a relative measurement error:

$$error = \frac{d_{measured} - d_{real}}{d_{real}} \tag{9}$$

where $d_{measured}$ is a calculated distance d_{real} is a real distance.

For comparison, the distance determination with using only the peak intensity (Fig. 5b) is presented. It increases linearly for all objects except the central one until the peaks of the pulses are distinguishable at a distance of about 60 centimeters between the objects. However, when peaks are distinguishable, the technology produces a minimal error, which indicates that there is no need to improve it and single-pixel imaging can be used only at peak points for visualization. When determining the distance from depth maps (Fig. 5a) the advantage of the technology is visible at distances less than 60 centimeters, since the error does not exceed 2.5% against 10% for the case of classical determination.

During simulation of FMCW LIDAR were used following parameters of radiation: $T \approx 3ms$ — modulation time of each signal, $f_0 = 0.5GHz$ — initial frequency, $B = 4.3GHz$ — chirp

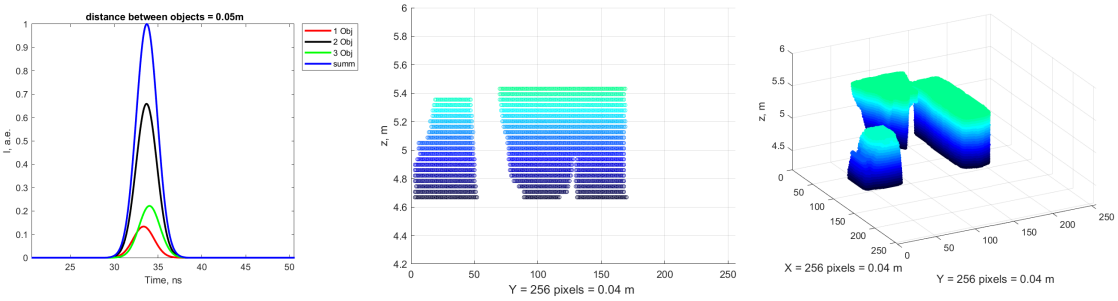

(a) (b) (c)

Fig. 3. The SPC TOF realisation based depth maps of three objects located at the distences 5m — square, 5.05m — rectangle, 5.1 m — triangle, (a) Temporal profile of the reflected signals, isometric (b) and side (c) view of depth maps constructed with single pixel images reconstructed using Hadamard patterns

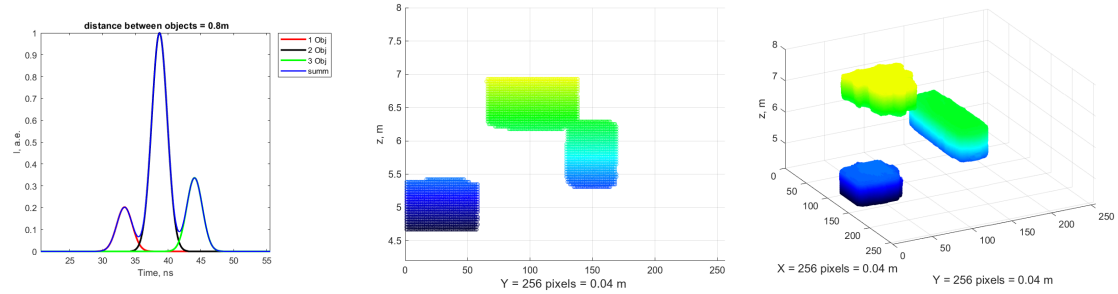

(a) (b) (c)

Fig. 4. The SPC TOF realisation based depth maps of three objects located at the distences 5m — square, 5.85m — rectangle, 6.6 m — triangle, (a) Temporal profile of the reflected signals, isometric (b) and side (c) view of depth maps constructed with single pixel images reconstructed using Hadamard patterns

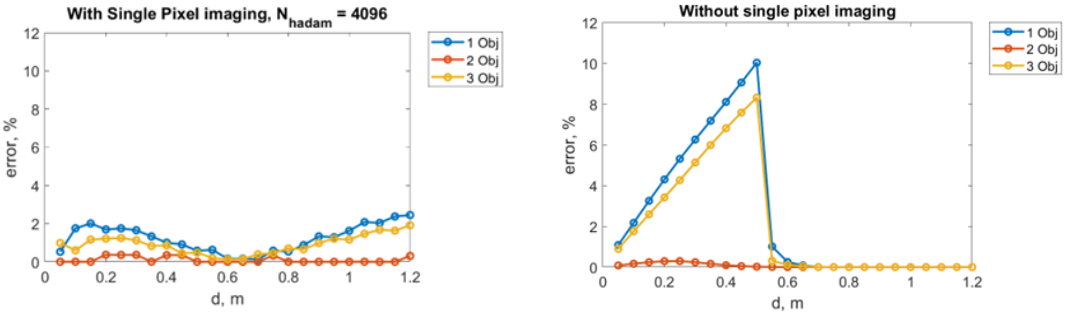

(a) (b)

Fig. 5. Relative error in distance determination via simulated TOF LIDAR, (a), with SPC and Hadamard patterns, (b) without SPC

bandwidth. Range resolution of FMCW LIDAR system can can be calculated as: $\delta R = \frac{c}{2B}$. After the Fourier transform, just B determines the position and width of the frequency peak, which directly affects the ability to recognize distances. The step between the frequencies is

approximately 0.03 MHz, which, when converted to a distance using B = 4300 MHz 0.07 m. To demonstrate the application of the single-pixel camera method using B = 4300 MHz frequency peak intensities marked with red dots correlate with information about objects located at a distance of 5 centimeters (Fig. 6). It indicates the possibility of improving the quality of distance determination, as in the case of TOF LIDAR, Despite the proximity of the frequency peaks, the single-pixel visualization method does not produce noise in the form of residual information about neighboring objects.

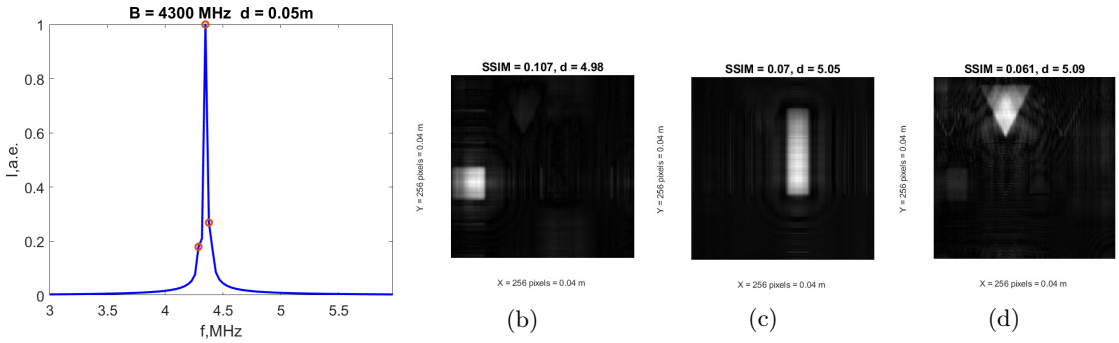

(a) (b) (c) (d)

Fig. 6. The SPC FMCW realisation (B = 4300MHz) with three objects at the distances 5m — square, 5.05m — rectangle, 5.1m — triangle: (a) Frequency spectrum of the reflected signals, (b), (c), (d) reconstructed images using Hadamard patterns

Conclusion

In this work, we explored the feasibility of integrating Time-of-Flight (TOF) and Frequency–Modulated Continuous–Wave (FMCW) LIDAR technologies with the single-pixel camera approach to enhance systems for generating three-dimensional depth maps of objects. The successful combination of LIDAR techniques with ghost imaging and the application of methods like compressive sensing to accelerate image acquisition has inspired further research into developing single-pixel LIDAR systems. While the use of single-pixel cameras for LIDAR applications has received limited attention, it shows promise for improving object image reconstruction at longer distances compared to ghost imaging.

The key result of this study is the simulation of the successful application of the single-pixel camera method to both FMCW and TOF LIDAR technologies to restore three-dimensional object maps. One important finding is the complementarity of these technologies: distance information obtained from LIDAR systems is crucial for image reconstruction through backward propagation. This confirms that three-dimensional single-pixel camera imaging relies on this data, highlighting avenues for the continued development of 3D single-pixel visualization.

Additionally, single-pixel imaging demonstrates improvements in LIDAR systems, particularly in visualizing objects that would otherwise be indistinguishable due to proximity. This is especially relevant in cases where frequency peaks merge in FMCW systems. In the simulations of SPC TOF and SPC FMCW systems, images of objects were successfully reconstructed even when the distance between them was small enough that the reflected signals became indistinguishable. For TOF LIDAR, this distance was less than 65 centimeters, demonstrating the system's ability to accurately locate objects based on compiled three-dimensional maps.

The successful integration of SPC TOF and SPC FMCW technologies demonstrated in this research opens new possibilities for enhancing remote sensing systems. It enables the visualization

of objects at greater distances than conventional TOF and FMCW LIDARs can achieve with similar technical performance. For FMCW LIDAR, SPC presents an appealing alternative to raster scanning, allowing for faster imaging. For TOF LIDAR, SPC offers an opportunity to improve accuracy without increasing the response time or cost of the receiver

Funding

Ministry of Education and Science of the Russian Federation (2019-0903).

References

[1] N.Jonnavithula, Y.Lyu, Z.Zhang, LiDAR Odometry Methodologies for Autonomous Driving: A Survey, 2021, arXiv preprint arXiv:2109.06120.

[2] G.Zhao, M.Lian, Y.Li, Z.Duan, S.Zhu, L.Mei, S.Svanberg, Mobile Lidar System for Environmental Monitoring, *Applied Optics*, **56**(2017), no. 5, 1506–1516. DOI: 10.1364/AO.56.001506

[3] F.Amzajerdian, V.E.Roback, A.Bulyshev, P.F.Brewster, G.D.Hines, Imaging Flash Lidar for Autonomous Safe Landing and Spacecraft Proximity Operation, in *AIAA SPACE 2016*, 2016, 5591. DOI: 10.2514/6.2016-5591

[4] T.Olvera Hale, Mapping and Navigation in an Unknown Environment Using LiDAR for Mobile Service Robots, 2020.

[5] D.Lee, M.Jung, W.Yang, A.Kim, LiDAR Odometry Survey: Recent Advancements and Remaining Challenges, *Intelligent Service Robotics*, **17**(2024), 1-24. DOI: 10.1007/s11370-024-00515-8

[6] B Behroozpour, P.A.Sandborn, M.C.Wu, B.E.Boser, Lidar system architectures and circuits, *IEEE Commun. Mag.*, **55**(2017), 135–142. DOI: 10.1109/MCOM.2017.1700030

[7] W.L.Chan, K.Charan, D.Takhar, K.F.Kelly, R.G.Baraniuk, D.M.Mittleman, A Single-Pixel Terahertz Imaging System Based on Compressed Sensing, *Applied Physics Letters*, **93**(2008), no. 12. DOI: 10.1063/1.2989126

[8] L.Leibov, A.Ismagilov, V.Zalipaev, B.Nasedkin, Y.Grachev, N.Petrov, A.Tcypkin, Speckle Patterns Formed by Broadband Terahertz Radiation and Their Applications for Ghost Imaging, *Scientific Reports* **11**(2021), no. 1, 20071. DOI: 10.21203/rs.3.rs-742925/v1

[9] J.Greenberg, K.Krishnamurthy, D.Brady, Compressive Single-Pixel Snapshot X-Ray Diffraction Imaging, *Optics Letters*, **39**(2014), no. 1, 111–114. DOI: 10.1364/OL.39.000111

[10] J.Ma, Single-Pixel Remote Sensing, *IEEE Geoscience and Remote Sensing Letters*, **6**(2009), no. 2, 199–203. DOI: 10.1109/LGRS.2008.2010959

[11] V.Studer, J.Bobin, M.Chahid, H.S.Mousavi, E.Candes, M.Dahan, Compressive Fluorescence Microscopy for Biological and Hyperspectral Imaging, *Proceedings of the National Academy of Sciences*, **109**(2012), no. 26, E1679–E1687. DOI: 10.1073/pnas.1119511109

[12] P.A.Morris, R.S.Aspden, J.E.C.Bell, R.W.Boyd, M.J.Padgett, Imaging with a Small Number of Photons, *Nature Communications*, **6**(2015), no. 1, 5913. DOI: 10.1038/ncomms6913

[13] J Cheng, Ghost Imaging through Turbulent Atmosphere, *Optics Express*, **17**(2009), no. 10, 7916–7921. DOI:10.1364/OE.17.007916

[14] Y.Bromberg, O.Katz, Y.Silberberg, Ghost Imaging with a Single Detector, *Phys. Rev. A*, **79**(2009), no. 5, 053840. DOI:10.1103/PHYSREVA.79.053840

[15] Z.Yang, Y.-M.Bai, K.-X.Huang, Y.-X.Liu, J.Liu, D. Ruan,J.-L.Li, Single-Pixel Full-Field Simultaneous Spatial and Velocity Imaging, *Optics and Lasers in Engineering*, **169**(2023), 107691.

[16] W.Zhang, Z.Cao, H.Zhang, H.Xie, Z.Ye, L.Xu, Distribution Retrieval of Both Depth and Reflectivity in 3-D Objects via Using Modulated Single Pixel Imaging, *IEEE Transactions on Instrumentation and Measurement*, **72**(2022), 1–11. DOI: 10.1109/TIM.2022.3224515

[17] X.Li, Y.Hu, Y.Jie, C.Zhao, Z.Zhang, Dual-Frequency Lidar for Compressed Sensing 3D Imaging Based on All-Phase Fast Fourier Transform, *Journal of Optics and Photonics Research*, **1**(2023). DOI: 10.47852/bonviewJOPR32021565

[18] G.M.Gibson, S.D.Johnson, M.J.Padgett, Single-Pixel Imaging 12 Years On: A Review, *Optics Express*, **28**(2020), no. 19, 28190–28208. DOI: 10.1364/OE.403195

[19] W.Gong, Performance comparison of computational ghost imaging versus single-pixel camera in light disturbance environment, *Optics & Laser Technology*, **152**(2022), 108140.

[20] B.Liu, P.Song, Y.Zhai, X.Wang, W.Zhang, Modeling and Simulations of a Three-Dimensional Ghost Imaging Method with Differential Correlation Sampling, *Optics Express*, **29**(2021), no. 23, 38879–38893. DOI:10.1364/OE.442889

[21] J.D.Schmidt, Numerical Simulation of Optical Wave Propagation with Examples in MATLAB, SPIE, 2010.

[22] B.Sun, M.Edgar, R.Bowman, L.Vittert, S.Welsh, A.Bowman, M.Padgett, 3D Computational Imaging with Single-Pixel Detectors, *Science (New York, N.Y.)*, **340**(2013), 844–847. DOI: 10.1126/science.1234454.

[23] Z.Zhang, X.Ma, J.Zhong, Single-Pixel Imaging by Means of Fourier Spectrum Acquisition, *Nature Communications*, **6**(2015), no. 1, 6225. DOI: 10.1038/ncomms7225

[24] W.-K.Yu, Super Sub-Nyquist Single-Pixel Imaging by Means of Cake-Cutting Hadamard Basis Sort, *Sensors*, **19**(2019), no. 19, 4122. DOI: 10.3390/s19194122

[25] M.-J.Sun, L.-T.Meng, M.P.Edgar, M.J.Padgett, N.Radwell, A Russian Dolls Ordering of the Hadamard Basis for Compressive Single-Pixel Imaging, *Scientific Reports*, **7**(2017), no. 1, 3464. DOI: 10.1038/s41598-017-03725-6

[26] X.Yang, Y.Zhang, C.Yang, L.Xu, Q.Wang, Y.Zhao, Heterodyne 3D Ghost Imaging, *Optics Communications*, **368**(2016), 1–6.

[27] D.J.Lum, S.H.Knarr, J.C.Howell, Frequency-Modulated Continuous-Wave LiDAR Compressive Depth-Mapping, *Optics Express*, **26**(2018), no. 12, 15420–15435. DOI: 10.1364/OE.26.015420

Моделирование метода однопиксельной визуализации для получения пространственного распределения объектов в ЛИДАР технологиях

Анастасия К. Лаппо-Данилевская
Азат О. Исмагилов
Университет ИТМО
Санкт-Петербург, Российская Федерация
Алексей А. Калиничев
Санкт-Петербургский государственный университет
Российская Федерация
Антон Н. Цыпкин
Университет ИТМО
Санкт-Петербург, Российская Федерация

Аннотация. В данной работе представлены результаты моделирования, демонстрирующие успешное применение однопиксельной визуализации для реконструкции трехмерных изображений объектов в сочетании с технологиями лазерных дальномеров. В частности, рассматривается интеграция методов лазерного дальномера с импульсным излучением на основе времени пролета (ToF) и частотно-модулированного непрерывного излучения (FMCW). В случае ToF моделирование показывает повышенную точность в различении расстояний между объектами, которые меньше расстояния, которое свет проходит за половину длительности сканирующего импульса. Эти результаты подчеркивают потенциал однопиксельной визуализации в современных приложениях трехмерной визуализации.

Ключевые слова: однопиксельная визуализация, трехмерная визуализация, лидары.